Received: 5 January 2022 | Revised: 17 March 2022 | Accepted: 1 April 2022

IET Power Electronics

DOI: 10.1049/pel2.12298

The Institution of Engineering and Technology WILEY

ORIGINAL RESEARCH

Analysis and design for constant current/constant voltage multi-coil wireless power transfer system with high EMF reduction

Zhichao Luo[1] | **Mehanathan Pathmanathan**[2] | **Wei Han**[3] | **Shuang Nie**[2] | **Peter W. Lehn**[2]

[1]Department of Engineering, Electrical Engineering Division, University of Cambridge, Cambridge, UK

[2]Department of Electrical Computer Engineering, Faculty of Applied Science and Engineering, University of Toronto, Toronto, ON, Canada

[3]Sustainable Energy and Environment Thrust, Function Hub, Hong Kong University of Science and Technology (Guangzhou), Qingsheng, Guangzhou, China

Correspondence
Zhichao Luo, Department of Engineering, Electrical Engineering Division, University of Cambridge, 9 JJ Thomson Avenue, CB3 0FA, Cambridge, UK.
Email: zhich.luo@utoronto.ca

Funding information
Natural Sciences and Engineering Research Council of Canada (NSERC), Grant/Award Number: CRDPJ513206-17

Abstract

The investigation on the constant current (CC)/constant voltage (CV) charging for the electric vehicle wireless power transfer (WPT) system has been widely conducted. However, the CC/CV performance under misalignment cases has been scarcely studied especially for the multi-coil WPT system. The resonant tank compensation methodology for the exciter-quadrature-repeaters (EQR) transmitter-based multi-coil WPT system is studied to achieve high power factor CC/CV charging with low leakage flux over ±150 mm lateral misalignment range. The EQR transmitter consists of one small exciter coil powered by a single full bridge inverter and two larger decoupled quadrature repeater coils which are magnetically coupled to the exciter coil. A variable switched capacitor is applied on the exciter side to maintain a high power factor in the CV mode. A 3-kW experimental setup with a 200 mm nominal vertical distance was built and a three-coil WPT system with a single large repeater coil is chosen as a comparison. Experimental results show that the EQR transmitter-based WPT system achieves 92% coil-to-coil efficiency and reduces the leakage flux density by 70% compared with the existing three-coil system in the CV mode at 150-mm lateral misalignment.

1 | INTRODUCTION

The promotion of electric vehicles (EVs) is of paramount importance to achieve transportation electrification. The widespread adoption of EVs places a great demand on the charging infrastructures. Wireless power transfer (WPT) as an emerging technology [1–3] has several unique advantages over conductive charging such as low electrocution risk and being highly attractive for autonomous charging. Several technical challenges must be resolved to ensure ubiquitous wireless charging in EVs. Lateral misalignment is an inevitable issue for vehicle parking. Compared with front-to-rear lateral misalignment, door-to-door lateral misalignment is more difficult for a driver to rectify and is the major challenge addressed in this paper. Associated with the lateral misalignment leakage magnetic field in the surrounding area is another concern. According to the SAE J2954 standard [4], there is a 27 μT (RMS) threshold for leakage magnetic flux density wherever people may be present. During the whole charging process of the lithium-ion battery, the battery pack equivalent load resistance, (ratio of the battery voltage and the DC charging current), may vary from a few ohms to several hundred ohms [5]. As such, several studies have proven that a load-independent constant current (CC)/constant voltage (CV) charging profile is preferable for lithium-ion batteries to ensure safety, durability, and high performance of the battery [6–9].

Multi-coil WPT systems, such as three-coil and four-coil WPT systems, have been widely investigated recently. In [10–13], multi-coil WPT systems, applying repeater or intermediate coils, have been proven to improve the transmission efficiency compared with the conventional two-coil systems [14]. In [15–20], the magnetic field distribution can be adjusted by controlling the current in each transmitter sub-coil in the multi-coil WPT systems in order to achieve high misalignment tolerance and low leakage magnetic field. In [18], a space vector-based excitation method was proposed in the bipolar transmitter pad

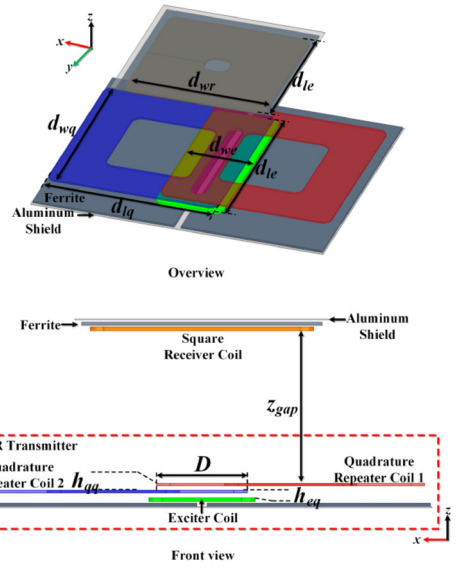

FIGURE 1 The structure of the EQR transmitter WPT system. EQR, exciter-quadrature-repeaters; WPT, wireless power transfer

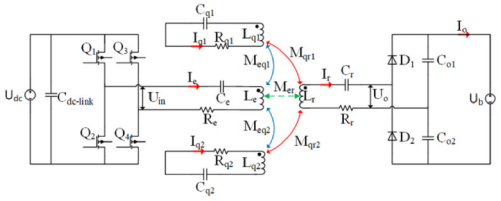

FIGURE 2 Equivalent electrical circuit of the EQR transmitter WPT system

and in [19] the current optimization method was developed for a three-coil decoupled transmitter. Both these methods in the multi-coil WPT systems allow the magnetic field to be oriented towards the receiver pad under lateral misalignment. However, each transmitter sub-coil has to be equipped with one inverter in these systems, resulting in an increase in system cost and control complexity.

In terms of CC/CV charging in multi-coil WPT systems, Li et al. [21] proposed a reconfigurable intermediate resonant circuit to implement CC/CV charging in a four-coil WPT system. In [22], hybrid compensation topologies on the receiver side were applied to allow a three-coil WPT system to achieve CC/CV charging. Yang et al. [23] utilized two different operation frequencies in a three-coil WPT system to achieve CC/CV charging in. However, the CC/CV performance for the multi-coil WPT systems under lateral misalignment was not considered in these previous studies. In [6], two different operation frequencies were applied in a four-coil WPT system and a closed-loop controller was developed in order to achieve CC/CV charging. However, the system could not maintain a zero phase angle (ZPA) between voltage and current at the inverter terminals in the misalignment cases, which results in higher power loss in the inverter. Besides, the EMF issue for the multi-coil WPT systems under the CC/CV mode in different misalignment cases has been scarcely studied in the previous literatures.

In this paper, a multi-coil WPT system, as shown in Figure 1, with an exciter-quadrature-repeaters (EQR) transmitter pad is proposed to efficiently achieve CC/CV charging. As shown in Figure 1, the EQR transmitter consists of a small exciter coil, and two magnetically decoupled big quadrature repeater coils. The exciter is energized by an inverter. As discussed in the previous work [24], the EQR transmitter WPT system can achieve CC and ZPA over ±150 mm lateral misalignment and ±20 mm vertical misalignment and the currents in the two quadrature repeater coils adjust autonomously based on the position of the receiver pad without any additional feedback control. Due to this attribute, the EQR transmitter WPT system has a large lateral misalignment tolerance and low EMF emission in the CC charging mode. In this paper, the investigation on CC/CV charging in the EQR transmitter WPT system is conducted while maintaining low EMF emission and ZPA over ±150 mm lateral misalignment considering 200 and 220 mm two vertical distances. The variable switched capacitor [25] is applied in the excitation resonant tank.

The main contributions of this paper are: (1) Load-independent CC/CV charging and ZPA conditions can be achieved simultaneously for the lateral misalignment of ±150 mm and vertical misalignment of +20 mm by applying the proposed coil topology and associated capacitor design methodology, without closed-loop control based on the output voltage or current signal from the receiver side. (2) Only one inverter unit is needed and the currents on two quadrature repeater coils adjust based on the receiver pad position without excitation current control on the transmitter side as required in [15, 17–19]. This current adjustment effectively reduces the leakage magnetic field in the lateral misalignment cases. The receiver coil is a simple rectangular coil and no additional component or control circuit is required on the receiver side.

In Section 2, the conditions required to achieve load-independent CC/CV charging and excitation coil ZPA are derived. Then in Section 3, two important design considerations are discussed in order to ensure the system operates efficiently in CC/CV charging mode within ±150 mm lateral misalignment. In Section 6, the design procedure of a 3-kW EQR transmitter WPT system is illustrated. Finally, in Section 5, a 3-kW experimental WPT system is presented and results are discussed to verify the system performance described in the above sections.

2 | CIRCUIT ANALYSIS OF THE EQR TRANSMITTER-BASED WPT SYSTEM

In this section, the conditions of the load-independent CC and CV charging are studied and the ZPA condition in each CC or CV mode is also derived. As shown in Figure 2, the equivalent electrical circuit of the EQR transmitter-based WPT system includes a dc power supply U_{dc}, a dc-link capacitor $C_{dc\text{-}link}$, a full-bridge inverter comprising Q_1–Q_4, four series compensated resonant tanks which include an exciter coil, two quadrature repeater coils, a receiver pad, and their associated series com-

pensation capacitors. On the receiver side, a voltage-doubling rectifier is used to connect the receiver pad to a battery.

2.1 | Constant current charging and zero phase angle conditions

To simplify the analysis of the proposed multi-coil WPT system, the fundamental harmonic approximation (FHA) is applied and the parasitic resistance of each resonant tank, namely R_e, R_{q1}, R_{q2}, and R_r is neglected. Furthermore, the dc power supply and the full-bridge inverter are simplified as an AC voltage source with the peak value U_{in} while the voltage doubling rectifier and the battery are converted into an equivalent resistance load. The equivalent resistance is determined by U_o shown in Figure 2, and the desired output power, P_o based on FHA and the fact that a voltage doubling rectifier is used.

$$R_E = \frac{U_o^2}{P_o} = \frac{2U_b^2}{P_o}. \tag{1}$$

where U_b is the battery voltage.

Based on Kirchhoff's voltage law, the proposed multi-coil system can be represented through a 4×4 matrix (all the parameters highlighted in bold are phasors in RMS in this paper)

$$\begin{bmatrix} \mathbf{U_{in}} \\ 0 \\ 0 \\ 0 \end{bmatrix} = \begin{bmatrix} Z_e & Z_{eq1} & Z_{eq2} & Z_{er} \\ Z_{eq1} & Z_{q1} & 0 & Z_{qr1} \\ Z_{eq2} & 0 & Z_{q2} & Z_{qr2} \\ Z_{er} & Z_{qr1} & Z_{qr2} & Z_r + R_E \end{bmatrix} \begin{bmatrix} \mathbf{I_e} \\ \mathbf{I_{q1}} \\ \mathbf{I_{q2}} \\ \mathbf{I_r} \end{bmatrix} \tag{2}$$

where Z_e, Z_{q1}, Z_{q2}, Z_r are the equivalent impedances of the four corresponding resonant tanks shown in Figure 2, and Z_{eq1}, Z_{eq2}, Z_{qr1}, Z_{qr2} are defined as the equivalent impedances of the mutual inductances between the coupled coils shown in Figure 2, respectively.

Since two quadrature repeater coils are designed to be decoupled, the mutual inductance between these two coils is assumed as zero in the second and the third rows of (2).

Therefore, all the impedances can be expressed as follows:

$$\begin{cases} Z_e = j\omega L_e + 1/j\omega C_e \\ Z_{q1} = j\omega L_{q1} + 1/j\omega C_{q1} \\ Z_{q2} = j\omega L_{q2} + 1/j\omega C_{q2} \\ Z_r = j\omega L_r + 1/j\omega C_r \\ Z_{eq1} = j\omega M_{eq1} \\ Z_{eq2} = j\omega M_{eq2} \\ Z_{qr1} = j\omega M_{qr1} \\ Z_{qr2} = j\omega M_{qr2} \\ Z_{er} = j\omega M_{er} \end{cases} \tag{3}$$

where $\omega = 2\pi f$ denotes the operation angular frequency; L_e, L_{q1}, L_{q2}, and L_r are the self-inductances of the exciter coil, the repeater coil 1, the repeater coil 2 and the receiver pad respectively; M_{er}, M_{eq1}, M_{eq2}, M_{qr1}, and M_{qr2} are the mutual inductances between the coupled coils shown in Figure 2, respectively.

Based on the matrix shown in (2), the corresponding voltage and current relationships can be achieved as

$$Z_{in} = \frac{U_{in}}{I_e} = \frac{A + BR_E + D}{-Z_{q1}Z_{q2}Z_r + Z_{qr1}^2 Z_{q2} + Z_{qr2}^2 Z_{q1} - Z_{q1}Z_{q2}R_E} \tag{4}$$

$$\frac{I_r}{U_{in}} = \frac{-Z_{eq1}Z_{qr1}Z_{q2} - Z_{eq2}Z_{qr2}Z_{q1} + Z_{er}Z_{q1}Z_{q2}}{A + BR_E + D} \tag{5}$$

where the symbol notations A, B, and D are expressed as

$$A = -Z_e Z_r Z_{q1} Z_{q2} + Z_r \left(Z_{eq1}^2 Z_{q2} + Z_{eq2}^2 Z_{q1} \right) + Z_e \left(Z_{qr1}^2 Z_{q2} + Z_{qr2}^2 Z_{q1} \right) - \left(Z_{qr1} Z_{eq2} - Z_{qr2} Z_{eq1} \right)^2 \tag{6}$$

$$B = -Z_e Z_{q1} Z_{q2} + Z_{eq1}^2 Z_{q2} + Z_{eq2}^2 Z_{q1} \tag{7}$$

$$D = -2Z_{er} \left(Z_{eq1} Z_{qr1} Z_{q2} + Z_{eq2} Z_{qr2} Z_{q1} \right) + Z_{q1} Z_{q2} Z_{er}^2 \tag{8}$$

It can be seen from (5) that $\mathbf{I_r}/\mathbf{U_{in}}$ is independent of the load resistance R_E when term B in (7) is equal to zero, which suggest that the CC charging mode condition is achieved if

$$Z_{e-cc} = \frac{Z_{eq1}^2 Z_{q2} + Z_{eq2}^2 Z_{q1}}{Z_{q1} Z_{q2}} \tag{9}$$

By substituting (9) into (4), the total input impedance is obtained

$$Z_{in} = \frac{U_{in}}{I_e} = \frac{A + D}{-Z_{q1}Z_{q2}Z_r + Z_{qr1}^2 Z_{q2} + Z_{qr2}^2 Z_{q1} - Z_{q1}Z_{q2}R_E} \tag{10}$$

If $\mathbf{Z_{in}}$ is real, ZPA is achieved. Given that both A and D are real, this requires the denominator of (10) to be real. This is satisfied if:

$$Z_{r-cc} = \frac{Z_{qr1}^2 Z_{q2} + Z_{qr2}^2 Z_{q1}}{Z_{q1} Z_{q2}} \tag{11}$$

If both (9) and (11) are satisfied, then (4) and (5) can be rewritten as the following equations. In this case, both CC and ZPA conditions can be simultaneously achieved in the proposed WPT system [24].

$$Z_{in} = \frac{U_{in}}{I_e} = \frac{A + D}{-Z_{q1}Z_{q2}R_E} \tag{12}$$

$$\frac{I_r}{U_{in}} = \frac{-Z_{eq1}Z_{qr1}Z_{q2} - Z_{eq2}Z_{qr2}Z_{q1} + Z_{er}Z_{q1}Z_{q2}}{A + D} \tag{13}$$

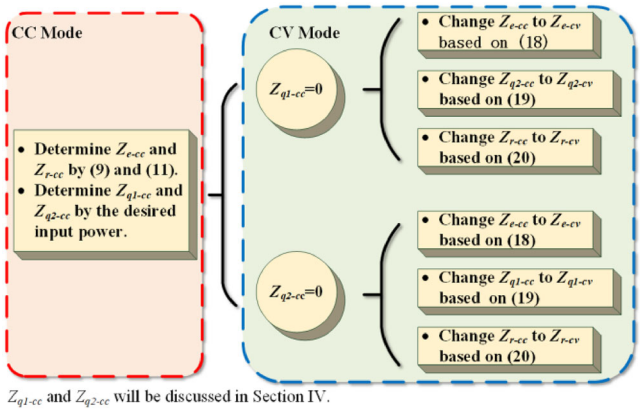

FIGURE 3 CC–CV mode operation schematic. CC–CV, constant current–constant voltage

2.2 | Constant voltage charging and zero phase angle conditions

For CV mode, the system output voltage U_o must be independent of the load R_E for a given input voltage U_{in}. According to (5), the ratio of $\boldsymbol{U_o}$ over $\boldsymbol{U_{in}}$ can be obtained as follows:

$$\frac{U_o}{U_{in}} = \frac{I_r R_E}{U_{in}} = \frac{\left(-Z_{eq1}Z_{qr1}Z_{q2} - Z_{eq2}Z_{qr2}Z_{q1} + Z_{er}Z_{q1}Z_{q2}\right) R_E}{A + BR_E + D} \tag{14}$$

The ratio becomes independent of R_E if $A + D$ can be assigned to zero. For $A + D = 0$

$$\frac{U_o}{U_{in}} = \frac{I_r R_E}{U_{in}} = \frac{-Z_{eq1}Z_{qr1}Z_{q2} - Z_{eq2}Z_{qr2}Z_{q1} + Z_{er}Z_{q1}Z_{q2}}{B}. \tag{15}$$

As shown in (15), $\boldsymbol{U_o}/\boldsymbol{U_{in}}$ is independent of R_E, which means the system can achieve load-independent CV charging. In terms of ZPA condition, the total input impedance of the system $\boldsymbol{Z_{in}}$ if $A + D = 0$ is provided by

$$Z_{in} = \frac{U_{in}}{I_e} = \frac{BR_E}{-Z_{q1}Z_{q2}Z_r + Z_{qr1}^2 Z_{q2} + Z_{qr2}^2 Z_{q1} - Z_{q1}Z_{q2}R_E} \tag{16}$$

Since term B is imaginary based on (7), $-Z_{q1}Z_{q2}R_E$ needs to be zero to ensure $\boldsymbol{Z_{in}}$ remains real and that ZPA is achieved. This requires $-Z_{q1}Z_{q2}R_E = 0$, which implies either $Z_{q1} = 0$ or $Z_{q2} = 0$.

Assuming Z_{q1} is assigned to zero,

$$A + D = Z_r Z_{eq1}^2 Z_{q2} + Z_e Z_{qr1}^2 Z_{q2} - \left(Z_{qr1}Z_{eq2} - Z_{qr2}Z_{eq1}\right)^2 - 2Z_{er}Z_{eq1}Z_{qr1}Z_{q2} \tag{17}$$

and three options to achieve $A + D = 0$

(1) Keep Z_{q2} and Z_r at the same values as in CC mode and then change Z_e to

$$Z_{e-cv} = \frac{\left(Z_{qr1}Z_{eq2} - Z_{qr2}Z_{eq1}\right)^2 + 2Z_{er}Z_{eq1}Z_{qr1}Z_{q2} - Z_{r-cc}Z_{eq1}^2 Z_{q2}}{Z_{qr1}^2 Z_{q2}} \tag{18}$$

(2) Keep Z_e and Z_r at the same values as in CC mode and then change Z_{q2} to

$$Z_{q2-cv} = \frac{\left(Z_{qr1}Z_{eq2} - Z_{qr2}Z_{eq1}\right)^2}{Z_{r-cc}Z_{eq1}^2 + Z_{e-cc}Z_{qr1}^2 - 2Z_{er}Z_{eq1}Z_{qr1}}. \tag{19}$$

(3) Keep Z_e and Z_{q2} at the same values as in CC mode and then change Z_r to

$$Z_{r-cv} = \frac{\left(Z_{qr1}Z_{eq2} - Z_{qr2}Z_{eq1}\right)^2 + 2Z_{er}Z_{eq1}Z_{qr1}Z_{q2} - Z_{e-cc}Z_{qr1}^2 Z_{q2}}{Z_{eq1}^2 Z_{q2}} \tag{20}$$

If Z_{q2} instead of Z_{q1} is assigned to be zero, then (18), (19), and (20) can be recalculated accordingly by using the same method.

Figure 3 shows the six different approaches to switch the system from CC mode to CV mode. To change mode, either Z_e, Z_q, or Z_r can be adjusted by adding a variable switched capacitor.

Since the ZPA is not beneficial for reducing the switching loss in the full-bridge inverter, it is preferred to adjust the impedances obtained from (18), (19), or (20) slightly in order to allow the system to be slightly inductive and achieve zero voltage switching (ZVS) other than ZPA in reality. This can be easily achieved as a variable switched capacitor is applied which is able to adjust its capacitance controlled by the DSP continuously.

Two questions need to be addressed to complete the design of this system, which are

(1) Which repeater resonant tank impedance, Z_{q1} or Z_{q2}, should be switched to zero for a given receiver pad position?

(2) Which impedance Z_e, Z_r, or the other repeater resonant tank impedance as per (18), (19), or (20) should be adjusted?

These two questions will be discussed in detail in the following section.

3 | DESIGN CONSIDERATIONS OF THE EQR TRANSMITTER-BASED WPT SYSTEM

3.1 | Zero-reactance resonant tank selection for CV mode

As discussed in the previous section, the first condition for the system to switch to the CV mode is to make $Z_{q1\text{-}cc} = 0$ or $Z_{q2\text{-}cc} = 0$, which means one of the repeater resonant tanks should be adjusted to be fully compensated. Based on the system matrix in (2), the currents in two repeater resonant tanks can be obtained

if the parasitic resistances in the resonant tanks are considered.

$$I_{q1} = \frac{-\left(Z_{eq1} I_e + Z_{qr1} I_r\right)}{Z_{q1} + R_{q1}} \tag{21}$$

$$I_{q2} = \frac{-\left(Z_{eq2} I_e + Z_{qr2} I_r\right)}{Z_{q2} + R_{q2}}. \tag{22}$$

where R_{q1} and R_{q2} are the parasitic resistances of two repeater resonant tanks.

From the above equations, it is seen that lower Z_{q1} or Z_{q2} values yield higher resonant tank currents. Therefore, the basic principle is to zero the reactance of the resonant tank with stronger coupling to the receiver pad. As such, the repeater coil with lower coupling to the receiver pad transfers lower power to the receiver pad and also causes lower leakage magnetic flux. If the mutual inductances between the receiver pad and two repeaters coil are equal (i.e. the receiver pad is close to the well-aligned case), the capacitor with the repeater coil placed closer to the exciter coil should be adjusted.

3.2 | Reactance adjustable resonant tank selection for CV mode

According to (18), (19), and (20), one of the impedances, Z_e, Z_r, or the non-zero Z_q value should be adjusted to allow the proposed system to switch into CV mode. This can be achieved by using a variable switched capacitor [25]. According to (18)–(20), there is the freedom to choose which resonant tank is compensated by the variable switched capacitor.

In practice, it is inevitable to have some discrepancy between the desired capacitor value and the actual capacitor value achieved by the variable switched capacitor. Therefore, the perturbation analysis of C_e, C_q, and C_r is conducted to investigate which tank capacitor should be controlled in order to achieve the ZPA condition during CV charging. In this analysis, all of the parasitic resistances in each resonant tank are taken into account. All the self-inductances, mutual inductances and parasitic resistances needed in this analysis are based on the experimental measurements, which are listed in Table 1.

In Figure 4, the results of the capacitance perturbation analysis in terms of the power factor are shown. The black lines display how the power factor changes in different lateral misalignment cases if (20) is applied and C_r has ±10% perturbation. The red and blue lines are the results when (19) and (18) are applied respectively. All of the calculations are obtained when the output power of the system is 3 kW and $R_E = 6.079\ \Omega$. According to the results, it can be seen that only if the variable switched capacitor is added in the exciter resonant tank does the system maintain unity power factor in each misalignment case despite there being a ±10% perturbation in C_e.

When it comes to the CV charging performance, the results are displayed in Figure 5. These two figures show the variation of the output voltage of the system in the well-aligned and the 150-mm misalignment cases, when the system equivalent load

TABLE 1 Design parameters of the EQR transmitter-based WPT system

Parameter	Value (mm)
Operation frequency (f_s)	85 kHz
Nominal vertical distance (z_{gap})[a]	200 mm
Exciter coil dimension ($d_{le} \times d_{we}$)[a]	185 × 410 (8 turns)
Receiver coil dimension ($d_{lr} \times d_{wr}$)[a]	325 × 325 (18 turns)
Quadrature repeater coil dimension ($d_{lq} \times d_{wq}$)[a]	390 × 410 (22 turns)
Overlap length of two repeater coils (D)	135
Two repeater coils dimension ($(2d_{lq}\text{-}D) \times d_{wq}$)[a]	645 × 410
Litz wire diameter in the exciter and receiver coil	6.53
Litz wire diameter in the repeater coils	3.75
Ferrite layer dimension in the EQR transmitter pad	670 × 550 × 5
Ferrite layer dimension in the receiver pad	350 × 350 × 5
Aluminium sheet dimension in the EQR transmitter pad	680 × 560 × 2
Aluminium sheet dimension in the receiver pad	370 × 370 × 2
Exciter coil to repeater coil 1 (b_{eq})[a]	15
Repeater coil 1 to repeater coil 2 (b_{qq})[a]	7

[a]These parameters are defined in Figure 1.

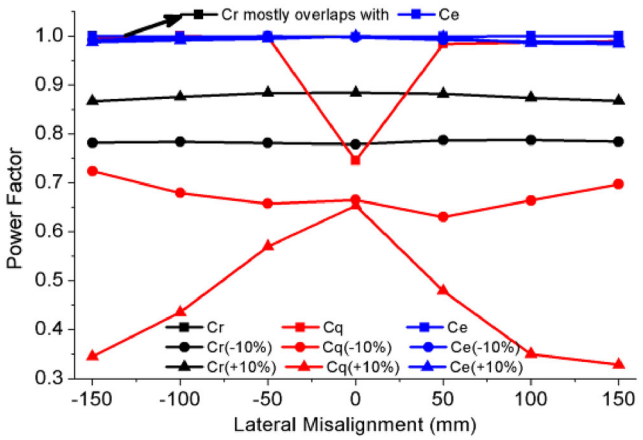

FIGURE 4 Capacitance perturbation analysis. (Power factor vs. lateral misalignment)

resistance increases from 6 Ω to 100 Ω. As can be seen in Figure 5, the CV output cannot be maintained by varying the capacitor in the repeater resonant tank when considering the parasitic resistances in the circuit. Meanwhile, it is clear that U_o has a considerable deviation from the desired value along with the increase of R_E with an adjustable capacitor on the receiver side when the capacitance value has a ±10% variation.

Based on the above studies, it is clear to conclude that: (1) the reactance of the resonant tank of the repeater having higher mutual inductance with the receiver pad should be switched to zero; (2) the variable switched capacitor should be added in the exciter resonant tank based on (18).

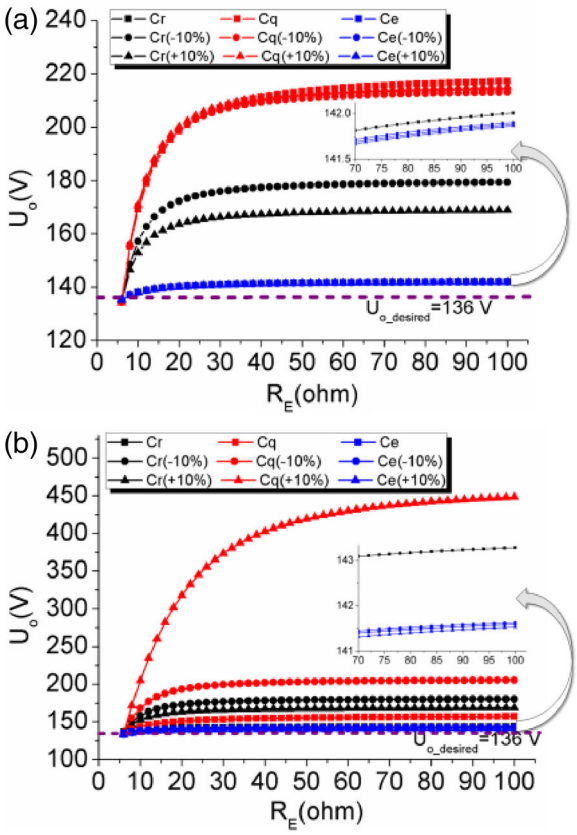

FIGURE 5 Capacitance perturbation analysis. (Output voltage vs. equivalent load resistance) (a) Well-aligned; (b)150-mm lateral misalignment

3.3 | Current of the proposed system in CV mode with variable switched capacitor in exciter resonant tank

The current distribution between the two repeater coils of the EQR transmitter-based WPT system is shown in Figure 6a in CV charging mode under different lateral misalignments. The inductance matrices for this simulation are based on the experiment measurement shown in Table 2. The impact caused by the lateral misalignment on the self-inductance in each resonant tank is minor due to the large air gap between the transmitter and the receiver pad. The mutual inductances between the repeater coils and the receiver pad are not identical in the well-aligned case because the two repeater coils are not in the same horizontal plane. Mutual inductances are equal at −25 mm, lateral misalignment is achieved by the FEA simulation. For comparison, the current in a single repeater of the existing three-coil WPT system from [23, 26, 27] is shown in Figure 6a. The operation principle of the existing three-coil system for CC/CV charging in this paper is similar to [23]. In the proposed system, the repeater coil with higher coupling to the receiver pad conducts much more current than the other repeater coil ($i_{q2} \gg i_{q1}$ for positive lateral misalignment). In Figure 6b, the repeater power loss is presented based on the current distribution in Figure 6a. The parasitic resistances of two repeater coils in the EQR system are 0.4 Ω for q1 and 0.36 Ω for q2, while the

TABLE 2 Inductance matrices of the EQR transmitter WPT system at z_{gap} = 200 mm

Parameter	Well-aligned (μH)	Misaligned +150 mm (μH)	Misaligned −150 mm (μH)
L_e	32.6	32.6	32.6
L_{q1}	267	268	267
L_{q2}	261	261	263
L_r	92.4	92.3	92.3
M_{eq1}	22.2	22.6	22.2
M_{eq2}	22.3	22.4	22.7
M_{qr1}	11.0	1.75	15.8
M_{qr2}	13.2	16.9	1.7
M_{er}	2.90	1.17	1.04
M_{qq}	1.30	2.08	2.03

L_e, L_{q1}, L_{q2}, L_r, M_{eq1}, M_{eq2}, M_{qr1}, M_{qr2}, M_{er} are defined in Figure 2.
M_{qq} is the mutual inductance between two quadrature repeater coils.

repeater coil in the three-coil system is 0.6 Ω. It can be seen that the proposed system achieves a 60% power loss reduction in the repeater coils in the extreme lateral misalignment cases when the system is in CV mode. In the well-aligned case, even though the current in one of the repeater coils in the EQR transmitter is greater than that in the repeater coil of the three-coil system, the power losses caused by the repeater coils are still slightly lower than that caused by the repeater of the three-coil system.

In terms of leakage magnetic field, this current distribution has a benefit in reducing the leakage flux density in the surrounding area especially when the receiver pad has a large lateral misalignment. In Figures 7c and 7d, the magnetic field distributions of the proposed system in both well-aligned and 150-mm misalignment cases are presented during CV charging. In comparison, the magnetic field distributions of the existing three-coil system in both well-aligned and 150-mm misalignment cases are also displayed in Figures 7a and 7b. As shown in Figures 7b and 7d, the leakage magnetic field on the left-hand side reduces significantly compared with the existing three-coil WPT system when the receiver pad has a 150-mm lateral misalignment towards the right-hand side owing to the proposed compensated capacitor selection methodology. When the receiver pad is at the well-aligned position, M_{qr2} is slightly higher than M_{qr1}. Therefore, the reactance in the repeater 2 resonant tank is set to zero resulting in most of the power being delivered through the repeater coil 2. In this case, the magnetic field distribution is also studied and shown in Figure 7c. In Figure 7a, it shows that the magnetic field distribution of the existing three-coil WPT system is symmetrical regarding the centre vertical line of the repeater when the receiver is in the well-aligned case. The magnetic field is more intensive around the repeater coil 2 than it is around the repeater coil 1 in Figure 7c. However, the safety-risk area where B_peak is greater than 38.2 μT in Figure 7c is similar to that of Figure 7a. This proves that this *B*-field asymmetry of the proposed system in the well-aligned case will

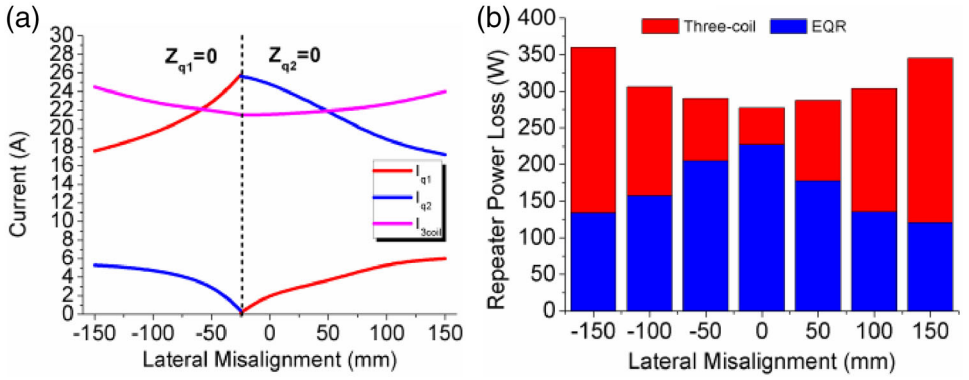

FIGURE 6 (a) Current distribution of the three-coil system and the EQR transmitter-based WPT system at z_{gap} = 200 mm; (b) power loss in two repeater coils of the EQR system and the repeater coil of the three-coil system

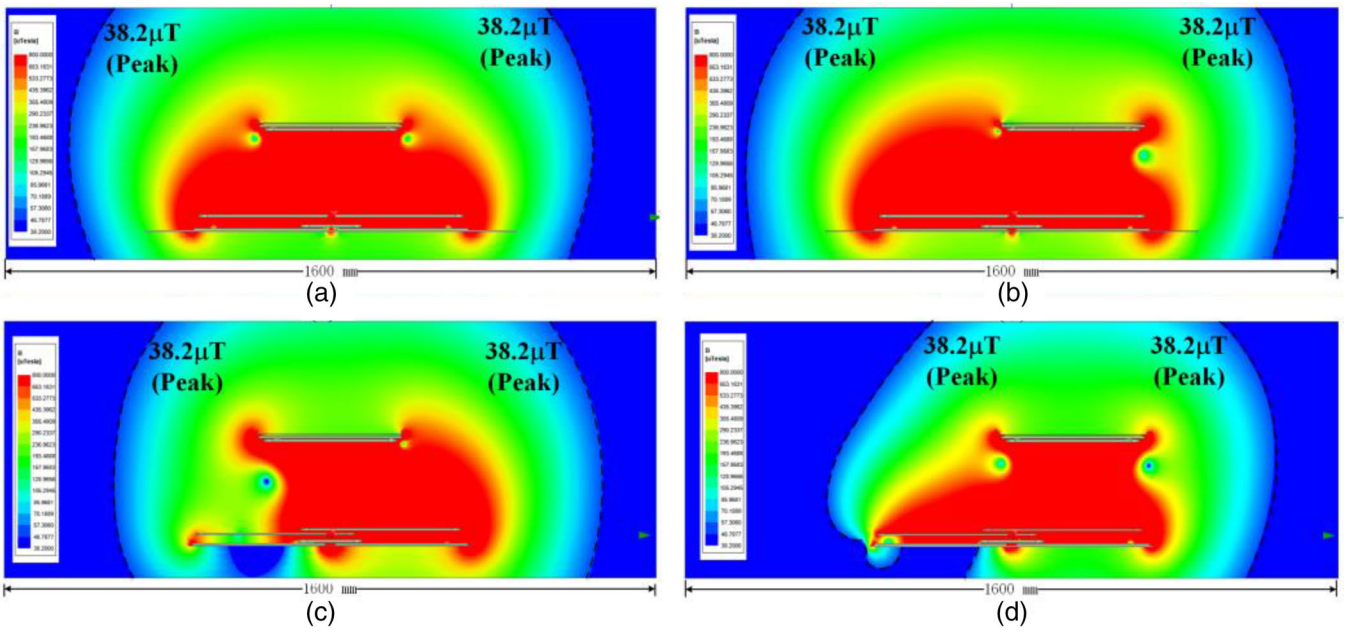

FIGURE 7 (a) Magnetic field distribution of the three-coil system in well-aligned case; (b) magnetic field distribution of the three-coil system in the 150-mm misalignment case; (c) magnetic field distribution of the EQR transmitter WPT system in well-aligned case; (d) magnetic field distribution of the EQR transmitter WPT system in the 150-mm misalignment case

not lead to a higher leakage magnetic field in the surrounding area.

3.4 | Principle of the variable switched capacitor circuit

As discussed in Section 3. A and B, the capacitors in both the exciter and the repeater resonant tanks should change their capacitances in order to implement CC versus CV charging. On the repeater side, the capacitor only needs to switch between two specific values for CC and CV modes; thus, two capacitors with a common electrical relay Relay1 or Relay2 in Figure 8 are added on each repeater coil. Since the voltage across $C_{q1\text{-}cc}$ or $C_{q2\text{-}cc}$ is much lower than the one across $C_{q1\text{-}cv}$ or $C_{q2\text{-}cv}$ during the system operation, these additional electrical relays will not increase too much cost.

A continuously variable capacitor is added to the exciter and is implemented using two MOSFETs, Q_{e1} and Q_{e2} as shown. Relay1, Relay2, Q_{e1} and Q_{e2} are open when the system is working in CC mode. When the battery management system or the control unit on the vehicle requires CV charging, one of the relays, Relay1 or Relay2, is switched on. As for the exciter side, according to (18), the capacitor value C_e should be adjusted once for every misalignment case in order to achieve ZPA condition and CV charging.

Therefore, the variable switched capacitor is applied which is shown in Figure 8a.

As shown in Figure 8a, the variable switched capacitor has another zero-crossing detection unit A2 that is used to avoid the

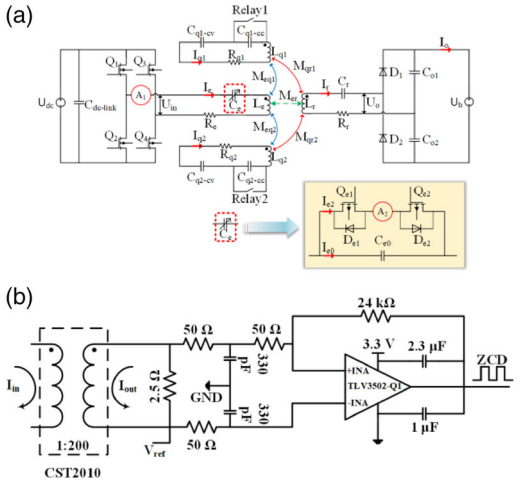

FIGURE 8 (a) Equivalent electrical circuit of the EQR transmitter WPT system with variable switched capacitor. (b) Schematic of the zero-crossing detection unit

current flowing into the body diode of the MOSFETs. Figure 8b shows that in the zero-crossing detection unit, an SMT current sense transformer CST2010 is used to scale down the measured current. Then the secondary scale-down current flows to the 2.5-Ω resistor to transfer the measured current to the AC voltage signal. The sampled AC voltage signal is compared to the reference voltage V_{ref} by using the rail-to-rail high-speed comparator TLV3502-Q1. Finally, the 3.3-V zero-crossing detection signal is transferred to the I/O pin of the digital signal processor (DSP).

In order to illustrate how to control the variable switched capacitor, the important signal waveforms are displayed in Figure 9. The first step is to implement a zero-crossing detection for I_e, which is shown as A_1 in Figure 8. The zero-crossing detection unit is used to monitor the rising edge and falling edge

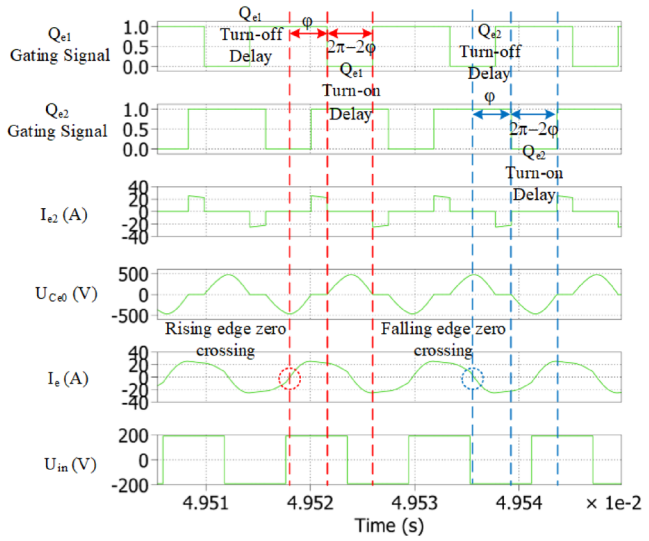

FIGURE 9 Waveform of the variable switched capacitor

zero-crossing of I_e. If the rising edge zero-crossing is detected, the timer in the DSP is triggered. Then, after $\frac{\varphi}{2\pi}T_s$ the MOSFET Q_{e1} turns off and it will turn on again after $\frac{2\pi-2\varphi}{2\pi}T_s$, where T_s is the switching period of the inverter. For Q_{e2}, the timer is triggered by the falling edge zero-crossing of I_e. Then, after $\frac{\varphi}{2\pi}T_s$ the MOSFET Q_{e2} turns off and it will turn on again after $\frac{2\pi-2\varphi}{2\pi}T_s$. By implementing the above-mentioned control scheme, the equivalent capacitance of the variable switched capacitor can be expressed as [25]

$$C_{eq} = C_{e0}\frac{1}{2-(2\varphi-\sin 2\varphi)/\pi}\left(\frac{\pi}{2}<\varphi<\pi\right). \quad (23)$$

The peak voltage stress of U_{ce0} can be calculated by the following equation which is derived in the Appendix.

$$U_{C_{p0}\_peak} = \frac{I_m}{\omega_0 C_{p0}}(\cos(\varphi)+1) \quad (24)$$

The desired C_{eq} can be calculated based on (18) in each misalignment case. That means an online mutual inductance detection unit is needed to obtain the control variable φ. There are several previous research works on measuring the mutual inductance in a WPT system by utilizing the voltage and current signal from the existing coils or adding the additional position sensing coils [28–31]. As such, the online mutual inductance detection unit is not within the scope of this paper as any of the aforementioned techniques could be applied.

4 | DESIGN AND OPERATION PROCEDURE OF A 3-KW EQR TRANSMITTER WPT SYSTEM

In this section, the design procedures of a 3-kW EQR transmitter WPT system is displayed including the CC mode and the CV mode respectively. The overall design process is summarized in Figure 10.

(1) Determine the desired total input impedance of the system in CC mode. The desired input rated power can be calculated by $P_{in} = P_o/\eta$ by assuming the coil-to-coil efficiency, η, is 94% and the DC output power is 3 kW. If the nominal input current, I_t^{rated} in Figure 8, is decided (i.e. 20 A in this paper), the total desired input impedance in the well-aligned case can be determined by $Z_{in-cc}^{desired} = P_{in}/(I_t^{rated})^2$ considering that the ZPA condition is satisfied.

(2) Apply the CC condition in (9) and ZPA condition in (11) to determine the impedance of the exciter and the receiver resonant tank $Z_{e\text{-}cc}$ and $Z_{r\text{-}cc}$ and the required compensation capacitor values C_{e0} and C_r (defined in Figure 8) can also be obtained accordingly.

(3) Assuming the symmetry, $Z_{q1} \approx Z_{q2}$ and, the value of Z_{q1} is given by (25) according to [24]. Then, the combined reactance of $C_{q1\text{-}cc}$ and $C_{q1\text{-}cv}$ in the upper repeater in Figure 8 and $C_{q2\text{-}cc}$

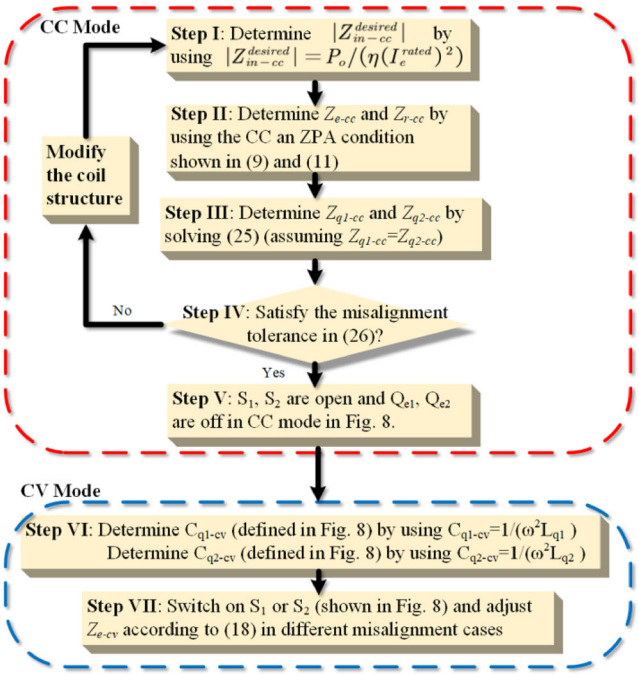

FIGURE 10 Design and operation procedures of the proposed WPT system

and $C_{q2\text{-}cv}$ in the bottom repeater in Figure 8 can be obtained.

$$Z_{q1} = \sqrt{\frac{\left(Z_{qr1}Z_{eq1} + Z_{qr2}Z_{eq2}\right)^2}{\left|Z_{in-cc}^{desired}\right| R_E}} \tag{25}$$

(4) If all the system parameters are chosen as stated in the previous procedures, then (26) is applied to check the system misalignment tolerance [24] in order to ensure the system still maintains the power factor higher than 0.9 within the prerequisite lateral misalignment (±150 mm in this paper). If (26) cannot be satisfied, the coil structure should be modified. Step I through Step IV would then be repeated. Once (26) is met, S_1, S_2 are switched off while Q_{e1}, Q_{e2} stay off allowing C_{e0} as the compensated capacitor for the exciter resonant tank.

$$\left|\frac{Z_{qr2}^2 + Z_{qr1}^2 - Z_{qr2}'^2 - Z_{qr1}'^2}{Z_{q1}R_E}\right| \le 0.48 \tag{26}$$

where Z'_{qr1} and Z'_{qr2} are the mutual impedances between two repeater coils and the receiver pad, respectively.

(5) $C_{q1\text{-}cv}$ and $C_{q2\text{-}cv}$ can be obtained by using $C_{q1\text{-}cv} = 1/(\omega^2 L_{q1})$ and $C_{q2\text{-}cv} = 1/(\omega^2 L_{q2})$.

(6) If the system switches to CV mode, turn on the switch in the repeater resonant tank which has the higher mutual inductance with the receiver pad. Adjust the impedance of the exciter resonant tank based on (18) by using the variable switched capacitor in different misalignment cases.

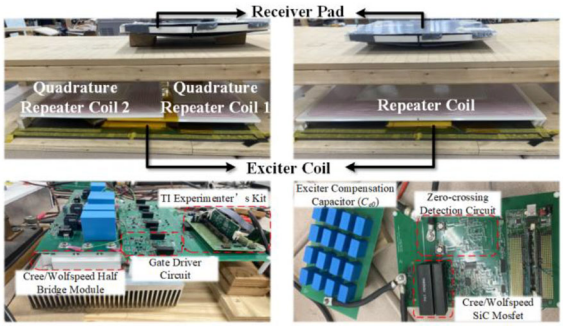

FIGURE 11 3-kW experiment setups of the EQR transmitter-based WPT system and the three-coil WPT system. (Both ferrite and aluminium shields are applied in the experiment on transmitter and receiver sides.)

5 | EXPERIMENT RESULTS AND DISCUSSION

In this section, a 3-kW experiment setup of the EQR transmitter-based WPT system was built in the lab and a 3-kW three-coil system was also built as a comparison. The EQR transmitter WPT system is shown in the upper left corner of Figure 11. The design parameters of the system are listed in Table 1 and the inductance matrices of the system in the well-aligned and the ±150 mm misalignment cases at z_{gap} = 200 mm are demonstrated in Table 2. In the upper right corner of Figure 11, there is a 3-kW experiment setup of the three-coil WPT system. In the three-coil system, the copper area of the repeater coil (650 mm × 410 mm with 22 turns) is similar to the overall copper areas of the two quadrature repeater coils in the EQR transmitter WPT system. The exciter coil and receiver pad are identical in these two systems. The vertical distance between the repeater coil and the exciter coil in the three-coil system is the same as the distance between the repeater coil 2 and the exciter coil in the EQR transmitter WPT system. In the bottom left corner of Figure 11 there is the inverter board which consists of two Cree/Wolfspeed CAS120M12BM2 SiC half bridge modules and a C2000™ DIMM100 Experimenter's Kit from Texas Instrument. In the bottom right corner of Figure 11, there is the variable switched capacitor board which includes two Cree/Wolfspeed C2M0025120D SiC Mosfets, two FFSH50120A 1.2 kV 50 A SiC Schottky diodes and a C2000™ DIMM100 Experimenter's Kit from Texas Instrument.

In the experiment, a variable resistive load is used so that the load condition can be adjusted to verify CC and CV modes. Besides the nominal z_{gap} = 200 mm, another z-plane, z_{gap} = 220 mm, is also tested to prove that the EQR transmitter-based WPT system can achieve the same performance at different vertical distances.

5.1 | ZPA and CC/CV condition verification

As shown in Figure 12a, when the receiver pad is in the well-aligned position at z_{gap} = 200 mm, the output voltage from

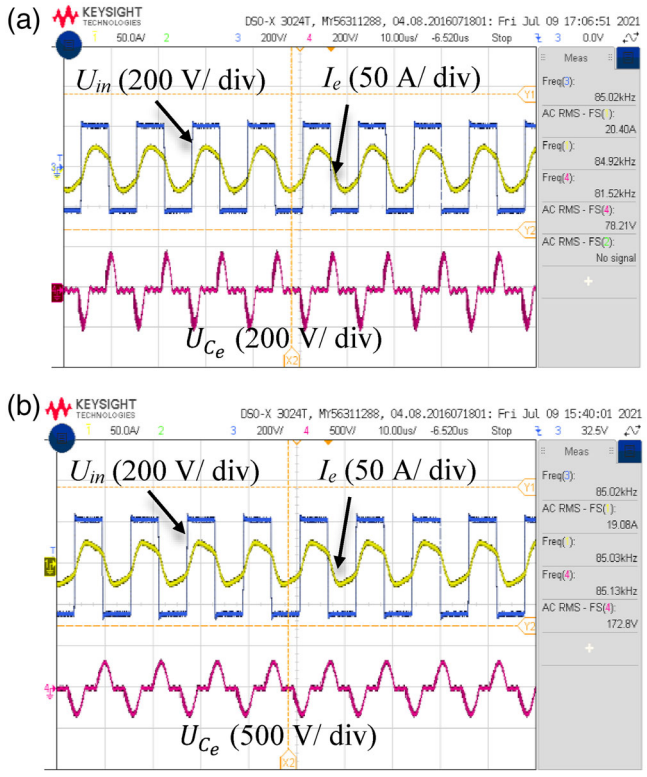

FIGURE 12 (a) Waveform in the well-aligned case at z_{gap} = 200 mm. (b) Waveform in the 150-mm misalignment case at z_{gap} = 220 mm. (Blue line: output voltage from the inverter; yellow line: current in the exciter coil; purple line: voltage across the variable switched capacitor C_e)

the inverter is in phase with the current in the exciter coil. In Figure 12b, when the receiver pad has a 150-mm misalignment at z_{gap} = 220 mm, the power factor on the exciter side is not exactly unity due to the parasitic resistance in each resonant tank. The exact C_e implemented by the variable switched capacitor is slightly higher than the desired one from (18). In this way, the system is inductive and the power factor remains higher than 0.9, which is essential for the inverter to achieve ZVS.

In order to verify the CC/CV performance of the proposed system, a variable resistive load is used to replace the battery load U_b shown in Figure 8. During the test, the load resistance R_L changes from 20 to 180 Ω and the nominal output power of 3 kW is achieved when the load is 30 Ω. The charging profiles in two different misalignment cases, namely well-aligned at z_{gap} = 200 mm and 150 mm misalignment at z_{gap} = 220 mm, are displayed in Figure 13. It can be seen from Figures 13a and 13c, the EQR transmitter-based WPT system achieves the desired CC/CV charging profile even though the receiver pad has lateral and vertical misalignments. In terms of the overall system efficiency, in CC mode, the efficiency is stable, which is around 91% in the well-aligned case and 86% in the misalignment case. In CV mode, as the resistance of the load increases, the efficiency decreases to 63.6% in the well-aligned case and 70% in the misalignment case when R_L = 180 Ω. Since it is close to the end of the charging process and the charging power is low, the relatively low system efficiency is still acceptable.

5.2 | System efficiency results

In this sub-section, the transmission efficiency from the exciter resonant tank to the receiver resonant tank (coil-to-coil efficiency) and the transmission efficiency from the DC input to the DC output (DC–DC efficiency) are studied in both the EQR transmitter WPT system and the three-coil system. Since it has already been proven that the EQR transmitter-based WPT system can achieve higher coil-to-coil efficiency and DC–DC efficiency compared with the three-coil system in [24] in CC mode, Figure 14 displays the comparison in CV mode at 3-kW output when the receiver pad is in two different z-planes. Overall, both the coil-to-coil efficiency and the DC–DC efficiency of the proposed system are higher than that of the three-coil system in CV mode. The highest coil-to-coil efficiencies for two different z-planes are achieved in the 150-mm misalignment case in the proposed system, which are 92% and 91.2% respectively. The reason why the efficiency increases as the lateral misalignment increases is that the system mostly relies on one quadrature repeater coil transferring power in the CV mode. As the receiver pad moves laterally towards one of those quadrature repeaters, the mutual inductance between the repeater coil and the receiver pad gets higher, which leads to higher transmission efficiency. The three-coil WPT system, shown in the upper right corner of Figure 11, has been proven to improve the transmission efficiency compared with the conventional two-coil system in several previous literatures such as [10, 12, 13, 26, 32]. The EQR transmitter-based WPT system shows further improvement in terms of transmission efficiency. Furthermore, the EQR transmitter WPT system can reduce the leakage flux density in the extreme lateral misalignment case in both CC and CV modes. The experimental results for the leakage flux density are discussed in the following sub-section.

In Figure 15, the power lower loss distribution in the EQR transmitter WPT system in both well-aligned at z_{gap} = 200 and 150 mm misalignment at z_{gap} = 220 mm is demonstrated. The major power loss is in the repeater coil 2 in both cases as it transfers the most of the power to the receiver side. The power loss in the exciter variable switched capacitor in the 150-mm misalignment case is higher than that in the well-aligned case. The reason for this is that in the well-aligned case, the turn-off time delay ' is longer than that in the 150-mm misalignment case in order to get a higher equivalent exciter capacitance. Therefore, the overlap area of the gating signals of Q_{e1} and Q_{e2} is bigger, which means less current flowing into the capacitor C_{e0} in the well-aligned case. However, the additional power electronics in the variable switched capacitor do not contribute significantly to the whole system power loss in both the well-aligned and the misalignment cases as seen from the exciter capacitor loss in Figure 15.

5.3 | Leakage flux density results

In CC mode, it has been proven that the proposed system achieves a 30% reduction of leakage flux density compared to

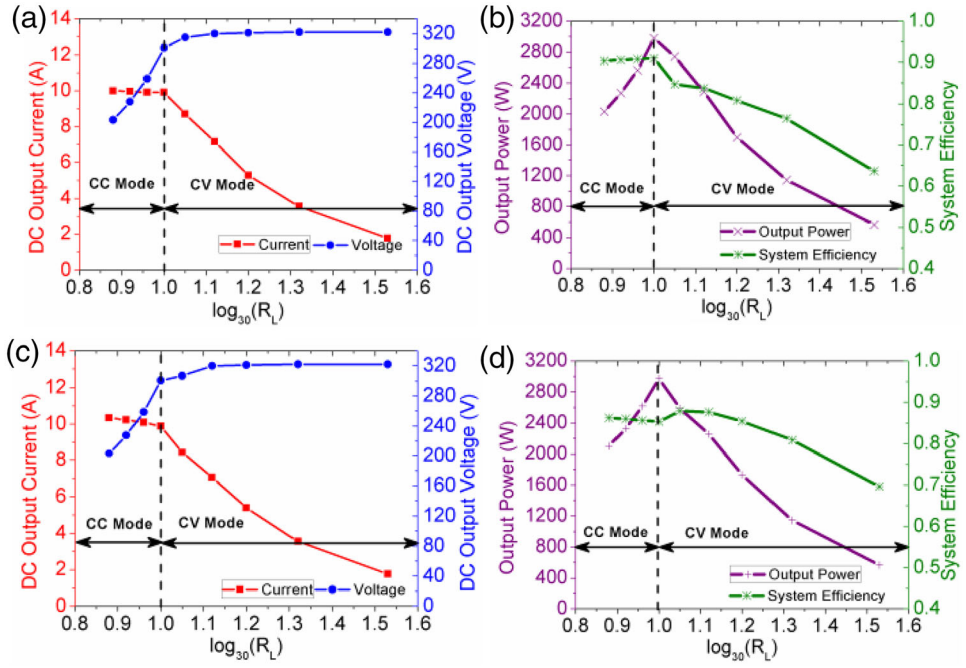

FIGURE 13 (a) Measured charging profile versus $\log_{30\text{the}}(R_L)$ in well-aligned case at z_{gap} = 200 mm. (b) Measured output power and system efficiency versus $\log_{30}(R_L)$ in the well-aligned case at z_{gap} = 200 mm. (c) Measured charging profile versus $\log_{30}(R_L)$ in 150-mm misalignment case at z_{gap} = 220 mm. (d) Measured output power and system efficiency versus $\log_{30}(R_L)$ in 150-mm misalignment case at z_{gap} = 220 mm

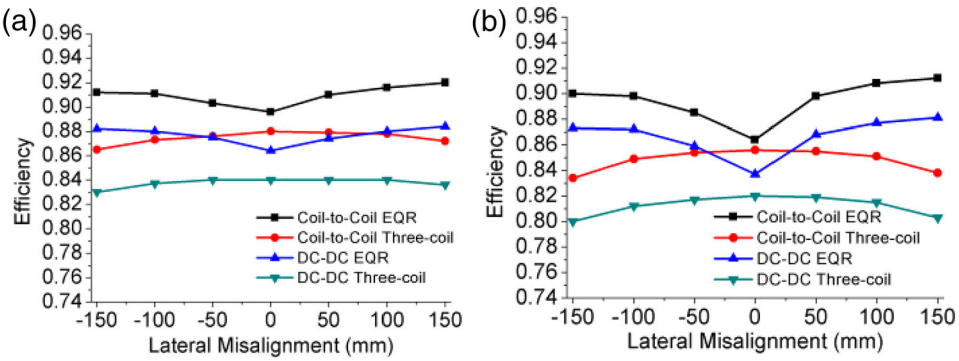

FIGURE 14 (a) System efficiency comparison between the EQR transmitter WPT system and the three-coil system at z_{gap} = 200 mm in CV mode. (b) System efficiency comparison between the EQR transmitter WPT system and the three-coil system at z_{gap} = 220 mm in CV mode

the three-coil system in the 150-mm lateral misalignment case in [24]. In this sub-section, the leakage magnetic flux density comparison between the EQR transmitter-based WPT system and the three-coil system is studied in CV mode at 3-kW output. In order to measure the leakage flux density in the surrounding area of the WPT system, three 800 mm×600 mm measurement planes are set, which are 800 mm away from the centre of the receiver pad as shown in Figure 16. This is representative of where a human could stand next to a vehicle. The method of achieving the maximum leakage flux density can be divided into three steps.

- Run the FEA simulation shown in Figure 16 in a specific receiver pad misalignment case.
- Plot the magnetic flux density distribution in those three measurement planes and find the worst-case point corresponding to the largest flux density in all measurement planes.
- A Hioki FT34700-50 MAGNETIC FIELD HiTESTER is used to measure the leakage flux density at the location of the worst-case point identified by the FEA simulation.

In these tests, two different vertical distances are considered, namely z_{gap} = 200 mm and z_{gap} = 220 mm. In terms of lateral misalignment, three cases, which are well-aligned, 150-mm misalignment and −150-mm misalignment, are taken into account. As a comparison, the leakage flux density of the three-coil system is also measured.

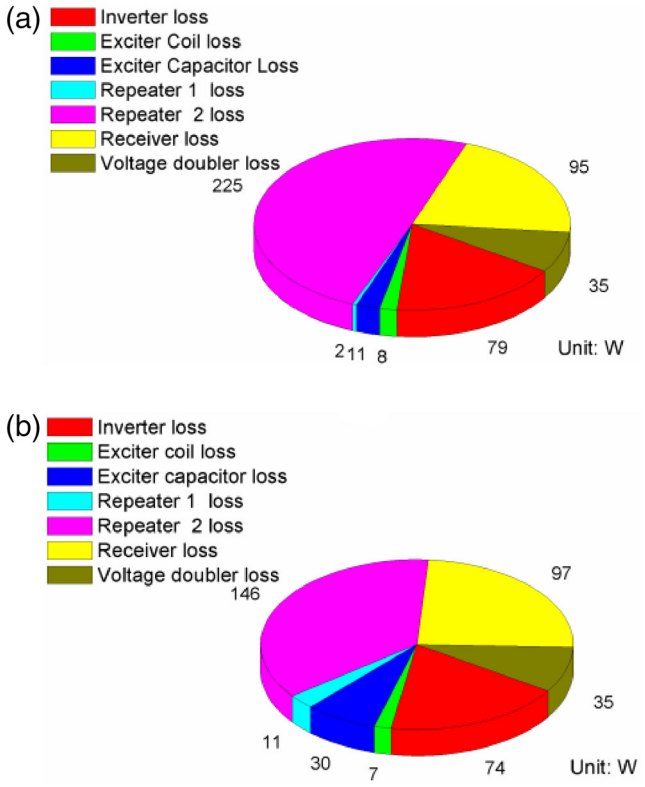

FIGURE 15 (a) Loss distribution of the EQR transmitter WPT system in the well-aligned case at z_{gap} = 200 mm in CV mode. (b) Loss distribution of the EQR transmitter WPT system in the 150-mm misalignment case at z_{gap} = 220 mm in CV mode

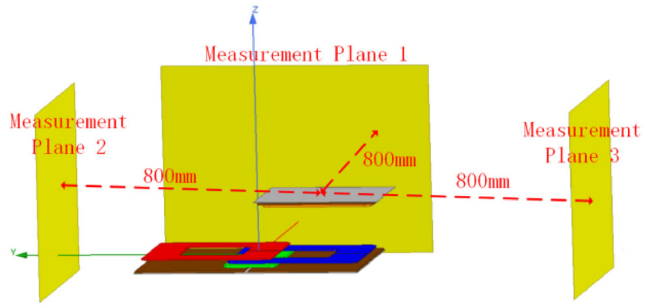

FIGURE 16 Schematic of the leakage measurement plane

As presented in Table 3, the leakage magnetic flux density of the EQR transmitter-based WPT system is slightly higher than the three-coil system in the well-aligned case, but it is still much lower than the safety limitation (27 μT) required by SAE J2954 [4]. In the extreme lateral misalignment case, the proposed system can significantly reduce the leakage magnetic field from 30.5 to 7.7 μT at z_{gap} = 220 mm. It is worth noticing that the leakage flux density of the three-coil system in the ±150 mm lateral misalignment cases at z_{gap} = 220 mm violates the safety limit 27 μT defined by the SAE J2954 [4]. Therefore, it can be concluded that the EQR transmitter-based WPT system can help reduce the leakage flux density in both CC and CV modes when the receiver has the lateral misalignment.

TABLE 3 Worst-case leakage flux density measurement results at 3-kW power transfer

Misalignment case	EQR (μT)	Three-coil (μT)	Leakage reduction
Well-align at z_{gap} = 200 mm	12.2	11.6	+5.2%
Well-align at z_{gap} = 220 mm	15.8	14.5	+8.2%
150 mm at z_{gap} = 200 mm	7.5	26.6	−71.8%
150 mm at z_{gap} = 220 mm	7.7	30.5	−74.8%
−150 mm at z_{gap} = 200 mm	8.5	26.4	−67.8%
−150 mm at z_{gap} = 220 mm	10.2	31	−67%

All the magnetic flux density measurements are in RMS.

6 | CONCLUSION

In this paper, an EQR transmitter pad is proposed and both CC and CV charging can be achieved by applying the presented resonant tank design method and the variable switched capacitor. Meanwhile, the whole system can also maintain ZPA condition while working in CC/CV mode. In CV mode, the repeater coil which has higher mutual inductance with the receiver pad transfers the majority of the power to the receiver side, which can effectively reduce the leakage flux density. When the receiver pad has high lateral misalignment this is especially significant as it allows charging to occur without exceeding the leakage flux safety threshold.

A 3-kW setup of the EQR transmitter-based WPT system was built in the lab. Based on the experimental results, the proposed system can perform a good CC/CV charging profile within ±150 mm lateral misalignment at two different vertical heights (z_{gap} = 200 and 220 mm). Compared with the three-coil WPT system, the EQR transmitter WPT system has a higher coil-to-coil and DC–DC efficiency when working in CV mode at 3-kW output. Furthermore, it is also verified that the EQR transmitter-based WPT system can reduce 70% of the leakage flux density in the 150-mm lateral misalignment case at the nominal vertical distance.

ACKNOWLEDGEMENT

This research was supported by the Natural Sciences and Engineering Research Council of Canada (NSERC), [funding Ref. No. CRDPJ513206-17]

CONFLICT OF INTEREST

All authors declare that they have no conflicts of interest.

DATA AVAILABILITY STATEMENT

The data that support the findings of this study are available from the corresponding author upon reasonable request.

ORCID

Zhichao Luo https://orcid.org/0000-0003-1133-7832
Mehanathan Pathmanathan https://orcid.org/0000-0002-2318-6712

Wei Han https://orcid.org/0000-0002-4544-2908
Shuang Nie https://orcid.org/0000-0002-5350-737X

REFERENCES

1. Ahmad, A., Alam, M.S., Chabaan, R.: A comprehensive review of wireless charging technologies for electric vehicles. IEEE Trans. Transport. Electrific. 4, 38–63 (2018).
2. Li, Y., Sun, W., Zhu, X., Hu, J.: A hybrid modulation control for wireless power transfer systems to improve efficiency under light-load conditions. IEEE Trans. Ind. Electron. 69(7), 6870–6880 (2021).
3. Li, Y., Liu, S., Zhu, X., Hu, J., Zhang, M., Mai, R., et al.: Extension of ZVS region of series–series WPT systems by an auxiliary variable inductor for improving efficiency. IEEE Trans. Power Electron. 36, 7513–7525 (2021).
4. Wireless power transfer for light-duty plug-in/electric vehicle and alignment methodology. ed: SAE TIR J2954_201906 (2019).
5. Buja, G., Bertoluzzo, M., Mude, K.N.: Design and experimentation of WPT charger for electric city car. IEEE Trans. Ind. Electron. 62, 7436–7447 (2015).
6. Tran, D.H., Vu, V.B., Choi, W.: Design of a high-efficiency wireless power transfer system with intermediate coils for the on-board chargers of electric vehicles. IEEE Trans. Power Electron. 33, 175–187 (2018).
7. Cong, Z., Jih-Sheng, L., Rui, C., Faraci, W. E., Ullah Zahid, Z., Bin, G., et al.: High-efficiency contactless power transfer system for electric vehicle battery charging application. IEEE Trans. Emerg. Sel. Topics Power Electron. 3, 65–74 (2015).
8. Vu, V.-B., Tran, D.-H., Choi, W.: Implementation of the constant current and constant voltage charge of inductive power transfer systems with the double-sided LCC compensation topology for electric vehicle battery charge applications. IEEE Trans. Power Electron. 33, 7398–7410 (2018).
9. Qu, X., Chu, H., Wong, S.-C., Tse, C.K.: An IPT battery charger with near unity power factor and load-independent constant output combating design constraints of input voltage and transformer parameters. IEEE Trans. Power Electron. 34, 7719–7727 (2019).
10. Moon, S., Kim, B.-C., Cho, S.-Y., Ahn, C.-H., Moon, G.-W.: Analysis and design of a wireless power transfer system with an intermediate coil for high efficiency. IEEE Trans. Ind. Electron. 61, 5861–5870 (2014).
11. Moon, S., Moon, G.-W.: Wireless power transfer system with an asymmetric 4-coil resonator for electric vehicle battery chargers. IEEE Trans. Power Electron. 31(10), 6844–6854 (2015).
12. Zhong, W.X., Zhang, C., Liu, X., Hui, S.Y.R.: A methodology for making a three-coil wireless power transfer system more energy efficient than a two-coil counterpart for extended transfer distance. IEEE Trans. Power Electron. 30, 933–942 (2015).
13. Zhong, W., Lee, C.K., Hui, S.Y.R.: General analysis on the use of tesla's resonators in domino forms for wireless power transfer. IEEE Trans. Ind. Electron. 60, 261–270 (2013).
14. Luo, Z., Wei, X.: Analysis of square and circular planar spiral coils in wireless power transfer system for electric vehicles. IEEE Trans. Ind. Electron. 65, 331–341 (2018).
15. Kim, S., Covic, G.A., Boys J. T.: Tripolar pad for inductive power transfer systems for EV charging. IEEE Trans. Power Electron. 32, 5045–5057 (2017).
16. Zaheer, A., Covic, G.A., Kacprzak D.: A bipolar pad in a 10-kHz 300-W distributed IPT system for AGV applications. IEEE Trans. Ind. Electron. 61, 3288–3301 (2014).
17. Pathmanathan, M., Nie, S., Yakop, N., P, W. Lehn: Field-oriented control of a three-phase wireless power transfer system transmitter. IEEE Trans. Transport. Electrific. 5, 1015–1026 (2019).
18. Pathmanathan, M., Nie, S., Yakop, N., Lehn, P.W.: Space-vector based excitation of a bipolar transmitter for wireless power transfer applications. IEEE Trans. Ind. Electron. 1 (2020).
19. Nie, S., Pathmanathan, M., Yakop, N., Luo, Z., Lehn, P.W.: Field orientation based three-coil decoupled wireless transmitter for electric vehicle charging with large lateral receiver misalignment tolerance. IET Power Electron. 14, 946–957 (2021).
20. Lin, F., Covic, G.A., Kesler, M.: Design of a SAE compliant multicoil ground assembly. IEEE Trans. Emerg. Sel. Topics Ind. Electron. 1, 14–25 (2020).
21. Li, Y., Hu, J., Liu, M., Chen, Y., Chan, K.W., He, Z., et al.: Reconfigurable intermediate resonant circuit based WPT system with load-independent constant output current and voltage for charging battery. IEEE Trans. Power Electron. 34, 1988–1992 (2019).
22. Li, Y., Xu, Q., Lin, T., Hu, J., He, Z., Mai, R.: Analysis and design of load-independent output current or output voltage of a three-coil wireless power transfer system. IEEE Trans. Transport. Electrific. 4, 364–375 (2018).
23. Yang, L., Li, X., Liu, S., Xu, Z., Cai, C., Guo, P.: Analysis and design of three-coil structure WPT system with constant output current and voltage for battery charging applications. IEEE Access 7, 87334–87344 (2019).
24. Luo, Z., Nie, S., Pathmanathan, M., Lehn, P.W.: Exciter-quadrature-repeaters transmitter for wireless electric vehicle charging with high lateral misalignment tolerance and low EMF emission. IEEE Trans. Transport. Electrific. 1-1 (2021).
25. Luo, Z., Zhao, Y., Xiong, M., Wei, X., Dai, H.: A self-tuning LCC/LCC system based on switch-controlled capacitors for constant-power wireless electric vehicle charging. IEEE Trans. Ind. Electron. 1-1 (2022).
26. Zhang, J., Yuan, X., Wang, C., He, Y.: Comparative analysis of two-coil and three-coil structures for wireless power transfer. IEEE Trans. Power Electron. 32, 341–352 (2017).
27. Kamineni, A., Covic, G.A., Boys, J.T.: Analysis of coplanar intermediate coil structures in inductive power transfer systems. IEEE Trans. Power Electron. 30, 6141–6154 (2015).
28. Chow, J.P.-W., Chung, H.S.-H., Cheng, C.-S.: Use of transmitter-side electrical information to estimate mutual inductance and regulate receiver-side power in wireless inductive link. IEEE Trans. Power Electron. 31, 6079–6091 (2016).
29. Yin, J., Lin, D., Parisini, T., Hui, S.Y.: Front-end monitoring of the mutual inductance and load resistance in a series–series compensated wireless power transfer system. IEEE Trans. Power Electron. 31, 7339–7352 (2016).
30. Gao, Y., Duan, C., Oliveira, A.A., Ginart, A., Farley, K.B., Tse, Z.T.H.: 3-D coil positioning based on magnetic sensing for wireless EV charging. IEEE Trans. Transport. Electrific 3, 578–588 (2017).
31. Lee, T.-S., Huang, S.-J., Dai, S.-H., Su, J.-L.: Design of misalignment-insensitive inductive power transfer via interoperable coil module and dynamic power control. IEEE Trans. Power Electron. 35, 9024–9033 (2020).
32. Ahn, D., Hong, S.: A study on magnetic field repeater in wireless power transfer. IEEE Trans. Ind. Electron. 60, 360–371 (2013).

How to cite this article: Luo, Z., Pathmanathan, M., Han, W., Nie, S., Lehn, P. W.: Analysis and design for constant current/constant voltage multi-coil wireless power transfer system with high EMF reduction. IET Power Electron. 1–14 (2022). https://doi.org/10.1049/pel2.12298

APPENDIX

Define the sinusoidal excitation current i_{Lf1} as follows

$$i_{Lf1} = I_m \sin(\omega_0 t) \tag{A1}$$

where I_m is the peak value of i_{Lf1} and ω_0 is the operation frequency of the inverter.

As shown in Figure 9, capacitor C_{p0} conducts current during the time interval [',$2\pi -$ ']. Therefore, the voltage C_{p0} across can be expressed as

$$U_{C_{p0}}(t) = \frac{1}{C_{p0}} \int_{t_d}^{t} I_m \sin(\omega_0 x)\, dx \tag{A2}$$

where $\omega_0 t_d =$' .

By solving the integral in (A2), the following equation can be obtained.

$$U_{C_{p0}}(t) = \frac{I_m}{\omega_0 C_{p0}} (\cos(\varphi) - \cos(\omega_0 t)) \tag{A3}$$

When $\omega_0 t = \pi$, $U_{C_{p0}}$ reaches to its maximum value.

$$U_{C_{p0\_peak}} = \frac{I_m}{\omega_0 C_{p0}} (\cos(\varphi) + 1) \tag{A4}$$